Chemical Engineering Journal 426 (2021) 131316

Contents lists available at ScienceDirect

Chemical Engineering Journal

journal homepage: www.elsevier.com/locate/cej

Desalination by direct contact membrane distillation using mixed matrix electrospun nanofibrous membranes with carbon-based nanofillers: A strategic improvement

Mohamed Essalhi [a,b], Mohamed Khayet [a,c,*], Solomon Tesfalidet [b], Mohammed Alsultan [b], Naser Tavajohi [b,*]

[a] Department of Structure of Matter, Thermal Physics and Electronics, Faculty of Physics, University Complutense of Madrid, Avda. Complutense s/n, Madrid 28040, Spain
[b] Department of Chemistry, Umeå University, Umeå 90187, Sweden
[c] Madrid Institute for Advanced Studies of Water (IMDEA Water Institute), Calle Punto Net N° 4, Alcalá de Henares, Madrid 28805, Spain

ARTICLE INFO

Keywords:
Dual-layered membranes
Triple-layered membranes
Electrospun nanofiber
Nanofillers protrusions
Electrospinning

ABSTRACT

Robust hydrophobic and superhydrophobic mixed matrix electrospun nanofibrous membranes (MM-ENMs) have been prepared from low- and high- molecular weight polyvinylidene fluoride with either multi-walled carbon nanotubes or graphene oxide nanofillers (0.05–0.5 wt%). The polymer solutions' properties, including their electrical conductivity, viscosity, and surface tension, were determined and used to guide the design of single-, dual-, and triple-layered MM-ENMs combining layers with different hydrophobic character. All MM-ENMs were subsequently prepared and characterized in terms of their morphology, hydrophobicity, mechanical properties, and direct contact membrane distillation (DCMD) performance. A thinner hydrophobic layer with a thicker hydrophilic support layer in dual-layered MM-ENMs reduced water vapor transport resistance and improved DCMD performance relative to single-layer MM-ENMs. Conversely, placing an intermediate hydrophilic layer between two hydrophobic layers in triple-layered MM-ENMs promoted water condensation (water pocket formation) and thus reduced DCMD performance. Over 10 h DCMD, the best-performing dual-layered MM-ENM allowed ultra-high permeate fluxes of up to 74.7 kg/m^2 h while maintaining a stable permeate electrical conductivity of around 7.63 μS/cm and a salt (NaCl) rejection factor of up to 99.995% when operated with a feed temperature of 80°C, a permeate temperature of 20°C, and a feed solution containing NaCl at a concentration of 30 g/L.

Abbreviations: DCMD, Direct contact membrane distillation; DFF, Differential filter flow; DL-MM-ENMs, Dual-layered mixed matrix ENMs; DMAC, N, N-dimethylacetamide; ENMs, Electrospun nanofibrous membranes; FESEM, Field emission scanning electron microscope; GO, Graphene oxide; HMPVDF, High molecular weight PVDF; IPA, Isopropyl alcohol; *LEP*, Liquid entry pressure (10^4 Pa); LMPVDF, Low molecular weight PVDF; MD, Membrane Distillation; MM-ENMs, Mixed matrix ENMs; MWCNs, Multi-Walled carbon nanotubes; NaCl, Sodium chloride; NF, Nanofiltration; PSF, Polysulfone; PVDF, Polyvinylidene fluoride; RO, Reverse osmosis; SL-MM-ENMs, Single-layered mixed matrix ENMs; SMMs, Surface Modifying Macromolecules; TEM, Transmission electron microscopy; TL-MM-ENMs, Triple-layered mixed matrix ENMs; μ_p, Viscosity (Pa s); C_{ffinal}, Final NaCl concentration in the feed (g L^{-1}); $C_{finitial}$, Initial concentration of NaCl in the feed (g L^{-1}); $C_{MWCNs,\chi p}$, Percolation threshold (vol%); C_{pfinal}, Final concentration of NaCl in the permeate (g/L); $C_{pinitial}$, Initial concentration of NaCl in the permeate (g L^{-1}); d_f, Fiber diameters (nm); d_i, Mean inter-fiber space (μm); E_b, Strain at break (%); J_w, Permeate flux (kg m^{-2} h^{-1}); M_w, Molecular weight (g.mol^{-1}); *PI*, Performance Index (kg.m^{-2}.h^{-1}); T_f, Feed temperature (°C); T_p, Permeate temperature (°C); T_S, Stress at break (MPa); w, Circulation stirring rate of the feed and the permeate (rpm); α, Salt rejection factor (%); δ, Thickness (μm); ε, Overall void volume fraction (%); θ, Contact angle (°); σ, Surface tension of polymer solution (mN m^{-1}); χ_p, Electrical conductivity of polymer solution (μS cm^{-1}).

* Corresponding authors: Department of Structure of Matter, Thermal Physics and Electronics, Faculty of Physics, University Complutense of Madrid, Avda. Complutense s/n, Madrid 28040, Spain (M. Khayet).
E-mail addresses: khayetm@fis.ucm.es (M. Khayet), naser.tavajohi@umu.se (N. Tavajohi).

https://doi.org/10.1016/j.cej.2021.131316
Received 10 April 2021; Received in revised form 29 June 2021; Accepted 11 July 2021
Available online 15 July 2021

1. Introduction

Membrane Distillation (MD) is a thermal separation process in which porous hydrophobic membranes are used as the separation media. A partial vapor pressure difference across the membrane is the driving force for mass transfer (i.e. vapor transport). MD is an attractive alternative to desalination technologies such as Reverse Osmosis (RO) and Nanofiltration (NF) because it can be performed using waste or renewable energy sources and it achieves excellent salt separation factors (and thus produces highly pure water) even when applied to strongly high salinity waters while operating at comparatively low hydrostatic pressures [1,2].

An ideal membrane for MD should have high liquid entry pressure (*LEP*), high hydrophobicity, low pore tortuosity, high void volume fraction (i.e. porosity), narrow pore size distribution; low thermal conductivity, antifouling properties (i.e. good scaling resistance), and overall robust for long-term operation [3]. Nanofibrous polymeric membranes with most of these properties have been prepared using physical, chemical, thermal, or electrostatic techniques. Sub-micrometer-sized polymeric electrospun nanofibrous membranes (ENMs) prepared by electrospinning are particularly attractive for MD because electrospinning is relatively inexpensive, highly flexible, and easy to organize different nanofibers into 3D networks with different thicknesses in spite of the instabilities of the electrified jet induced by the established electric field. Over the last decade, several groups have reported on the production of hydrophobic ENMs using hydrophobic polymers such as fluoropolymers [4–8].

Various strategies have been proposed to improve the properties and efficiency of direct contact membrane distillation (DCMD) membranes. These include coating with hydrophobic nanoparticles [9–13], the use of Surface Modifying Macromolecules (SMMs) [8,14,15], blending [16–18], incorporating nanofillers [19–22], and using dual and triple-layered with hydrophobic/hydrophilic structures [23–29]. It was reported that these dual- and triple-layered membranes exhibit better DCMD performance than single-layered hydrophobic ENMs of the same thickness [9,23–25,30]. The DCMD performance of dual-layered hydrophobic/hydrophilic membranes depends on the properties of the thin hydrophobic layer and the thicker hydrophilic support layer with bigger pores that provides the necessary mechanical strength and reduces both the heat loss by conduction and temperature/concentration polarization effects [26,31,32].

Nanofibrous membranes containing carbon-based nanofillers such as carbon nanotubes (CNTs) and graphene have been studied extensively in DCMD desalination in recent years because of their excellent thermal, chemical, and mechanical properties, which are due in large part to the exceptionally high aspect ratios and low densities of these nanofillers [20,22,29,33–39]. In this study, we combine the two above-mentioned strategies to prepare single-layered (SL), dual-layered (DL), and triple-layered (TL) mixed matrix electrospun nanofibrous membranes (MM-ENMs) using multi-walled carbon nanotubes (MWCNs) and graphene oxide (GO) as nanofillers. The used hydrophobic polymer was polyvinylidene fluoride (PVDF) and both high molecular weight PVDF (HMPVDF, M_w = 275,000 g/mol) and low molecular weight PVDF (LMPVDF, M_w = 180,000 g/mol) were tested. The two nanofillers (MWCNs and GO) were evaluated independently at different concentrations 0.05, 0.1, 0.15, 0.2, 0.25, and 0.5 wt% in HMPVF and LMPVDF polymer solutions. Initially, single-layered MM-ENMs (SL-MM-ENMs) were prepared and tested to determine their DCMD performance. The best performing SL-MM-ENM was then considered as a basis for the development of dual-layered (hydrophobic/hydrophilic and hydrophobic$^+$/hydrophobic$^-$ layers having different hydrophobic character) ENMs and triple-layered (hydrophobic/hydrophilic/hydrophobic and three layers with different hydrophobic level hydrophobic$^+$/hydrophobic$^-$/hydrophobic$^+$) ENMs. The hydrophilic layer of these ENMs was prepared using polysulfone (PSF) polymer and the DCMD desalination performance of all electrospun membranes was evaluated.

Experiments were conducted to study the effects of the loadings of MWCNs and GO on the properties of the LMPVDF and HMPVDF polymer solutions and the nanofiber structure, morphology, hydrophobicity, wettability, mechanical properties, and desalination performance of the electrospun MM-ENMs. For comparative purposes, pristine LMPVDF and HMPVDF ENMs without nanofillers (SL-0-LMPVDF and SL-0-HMPVDF) were also prepared under the same conditions as those containing nanofillers (MM-ENMs). For dual-layered MM-ENMs, the thickness of the hydrophilic layer was varied by changing the electrospinning time while keeping all other conditions unchanged. Additionally, different triple-layered MM-ENMs were prepared by changing the nature of the middle layer while keeping the electrospinning time (i.e. thickness) of the top and bottom layers the same.

2. Results and discussion

2.1. Characterization and DCMD performance of single-layer membranes (SL-MM-ENMs)

2.1.1. Morphology and hydrophobicity

Figs. 1 and 2 show FESEM images of LMPVDF and HMPVDF SL-MM-ENMs prepared with different concentrations of MWCNs or GO as nanofillers. It is well known that the properties of the electrospinning polymer solution (in particular its surface tension, viscosity, and electrical conductivity) strongly affect the morphological structure of ENMs [40–42]. The main solution properties governing the formation of beaded and beads-on-string nanofibers are the viscosity, electrical conductivity, and surface tension. A higher viscosity promotes the formation of thick fibers; a higher electrical conductivity favors the formation of thinner fibers, while a high surface tension promotes bead formation.

FESEM images of SL-MM-ENMs prepared with LMPVDF (Fig. 1) show nanofibrous networks with no particular orientation in any direction (i.e. entangled fibers). Adding nanofillers to the LMPVDF polymer solution had two distinct effects with opposing impacts on the size of the electrospun nanofibers: the nanofillers increased the solution's viscosity, favoring the formation of thicker nanofibers, but also increased its electrical conductivity, favoring thinner nanofibers. When percolation pathways is formed in an electrospinning polymer solution, the former effect dominates at lower nanofiller concentrations, but the latter effect becomes increasingly important at higher nanofiller concentrations. Adding 0.1 wt% of MWCNs or GO to the LMPVDF polymer solution increased the diameter of the resulting nanofibers by 27% and 47%, respectively; indicating that the increase in the viscosity of the polymer solution was dominant and that this effect was much more pronounced with GO than with MWCNs. (See SI, Fig. S1e). Increasing the solution's nanofiller content above 0.1 wt% resulted in smaller nanofibers. This is consistent with previous reports and indicates that the increase of the electrical conductivity becomes more important as the nanofiller content is enhanced [40,43].

Fig. 2 and Table S1 show FESEM images of the SL-MM-ENMs prepared with HMPVDF. In this case, adding nanofillers to the electrospinning polymer solution had the opposite effect on fiber diameter to that seen with LMPVDF. For low to moderate nanofiller contents between 0.05 wt% and 0.25 wt%, the nanofiber diameter generally declined as the nanofiller content was increased; the nanofiber diameters of SL-MM-ENMs containing 0.25 wt% of MWCNs or GO were 66.7% and 55.3% lower, respectively; than that for ENMs electrospun without nanofillers. The nanofiller-induced an enhancement of the polymer solution's electrical conductivity, thus dominated under these conditions, and this effect was more pronounced for MWCNs than for GO (see Fig. S1b and c). However, raising the nanofiller concentration from 0.25 wt% to 0.5 wt% caused the fiber diameter to increase from 310 nm to 439 nm for MWCNs and from 418 nm to 536 nm for GO. The nanofiller induced an increase of the viscosity of the polymer solutions, thus became stronger at the highest nanofiller contents, and this effect was

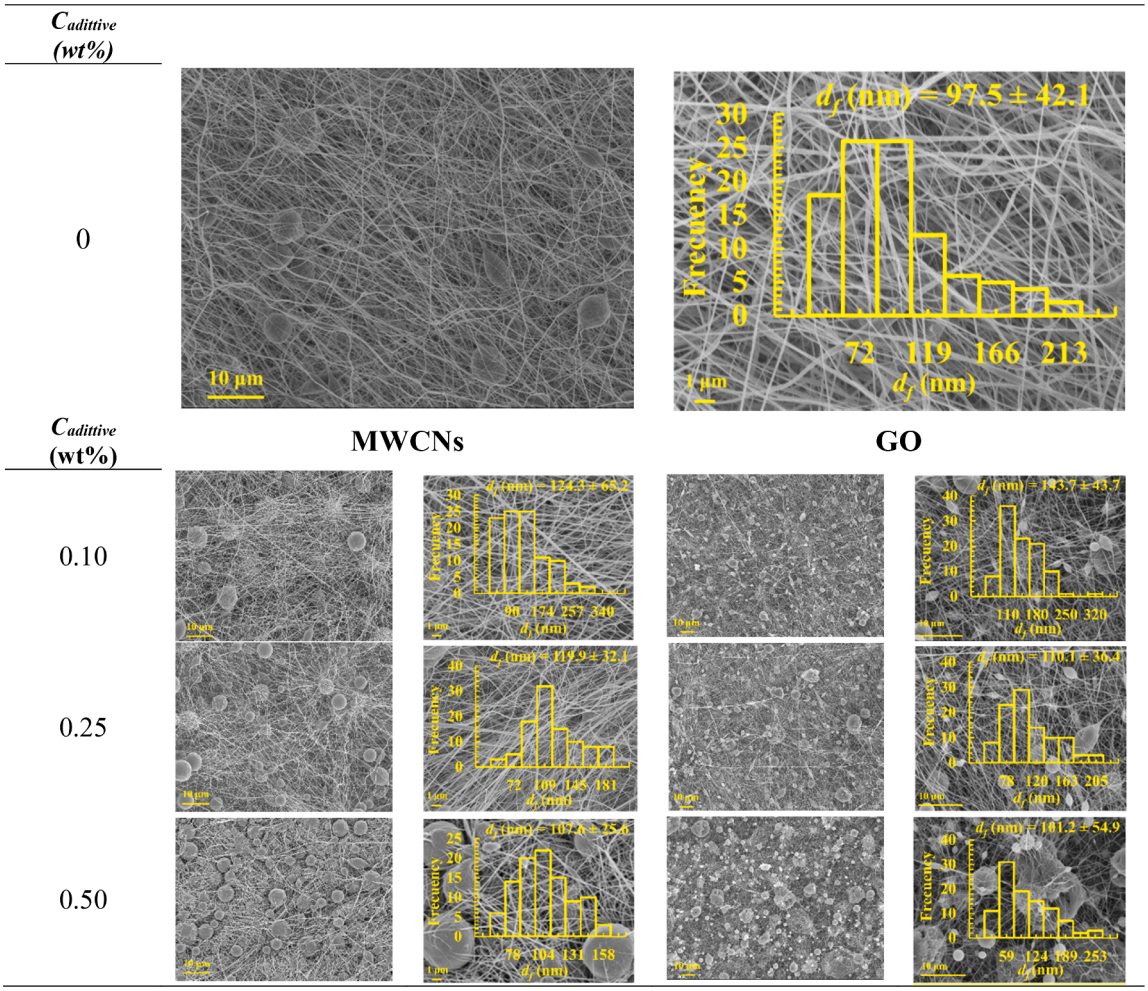

Fig. 1. FESEM images of the surfaces of SL-MM-ENMs prepared from LMPVDF solutions having different contents of MWCNs and GO together with histograms showing their nanofiber diameter (d_f) distributions.

more pronounced for GO than for MWCN (see Fig. S1e).

Figs. 1 and 2 show the relative abundance of beaded and interwoven fibers with beads-on-string morphologies with the increase of the nanofiller concentration. This can be attributed to the increase of the surface tension and electrical conductivity of the polymer solutions caused by the nanofillers. When the surface tension is high, the electrospinning jets form spheres (i.e. beads) to minimize their surface free energy [44,45]. In addition, increasing the electrical conductivity of the polymer solution increases the solution jet's surface charge density [44,45], causing its elongation in response to the applied electrical field. Both favor the formation of beaded networks with thin nanofibers.

The beads-on-string morphology was especially prominent in systems with a nanofiller content of 0.5 wt% because of their high surface tension and the agglomeration of the nanofillers during nanofiber formation (Figs. 1 and 2). The degree of bead formation was more significant in MWCN-containing nanofibers than in those containing GO, especially for nanofillers concentrations greater than 0.25 wt%. This may be partially due to the structural differences between the nanotubes and the GO nanosheets. When the GO content was high, the high surface tension of the polymer solution induced jet instability that adversely affected the electrospinning process and favored the formation of spray droplets, leading to the creation of entangled nanofibers. This phenomenon was especially pronounced when the GO content was above 0.25 wt%.

The surface morphology of the prepared SL-MM-ENMs was characterized by the presence of several beads, hills, and valleys, indicating micro- and nano-scale roughness that would be expected to increase surface hydrophobicity [46]. Accordingly, the contact angles of all SL-MM-ENMs were above 135° (see Fig. 3a and b, and Table S1). Superhydrophobicity (i.e. a contact angle above 150°) was observed in SL-MM-ENMs prepared from LMPVDF and HMPVDF with GO and MWCN contents above 0.25 wt%, respectively. Similar results were obtained in a previous reported study for graphene containing electrospun nanofibers [47]. Additionally, when comparing SL-MM-ENMs electrospun using the same nanofiller content and PVDF molecular weight, the surface of the membranes containing GO were more hydrophobic than those containing MWCNs. This can be explained based on TEM images of SL-MM-ENMs shown in Fig. 3c. Various structural features arising from the presence of the nanofillers can be seen in the fibers, including protrusions and agglomerations as well as entangled nanofillers and the differing alignments of the nanofillers relative to the nanofiber axis. Most of the visible MWCNs have curved or wavy rather than straight conformations. Previous studies have found that MWCNs are quite susceptible to disturbances during electrospinning, resulting in disordered orientations along the nanofiber axis [48,49]. The TEM images of SL-MM-ENMs containing GO show irregularly arranged protrusions and agglomerations. The protrusions appear to be more pronounced than those originating from MWCNs, resulting in greater nano-surface roughness and hydrophobicity. In general, these results support the conclusion that incorporating carbon-based nanofillers into polymer solutions is an attractive strategy for preparing MD membranes with superhydrophobic surfaces.

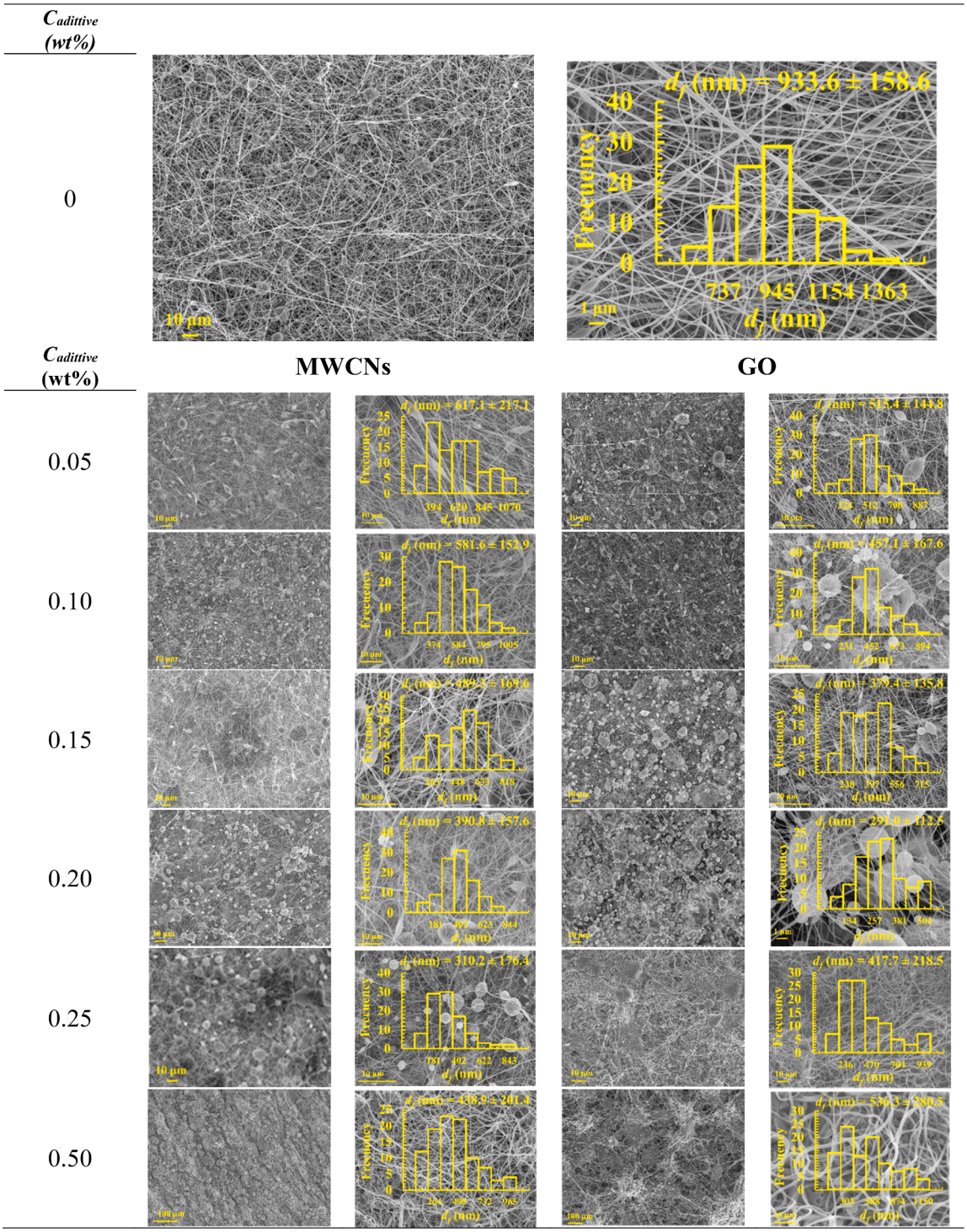

Fig. 2. FESEM images of the surfaces of SL-MM-ENMs prepared from HMPVDF solutions with different contents of MWCNs and GO together with histograms showing their nanofiber diameter (d_f) distributions.

2.1.2. Void volume fraction, Inter-fiber space, and liquid entry pressure

Membrane properties with important effects on MD performance include the void volume fraction (ε), the mean inter-fiber space (d_i) and inter-fiber space distribution (PSD), and the liquid entry pressure (*LEP*). It is generally accepted that a higher void volume fraction induces a higher MD permeate flux by increasing the membrane's surface area per unit volume. The presence of voids also reduces the heat loss by conduction during MD because the thermal conductivity coefficients of gases trapped inside the membrane pores are an order of magnitude lower than that of the membrane matrix [50].

Fig. 4a and b and Table S1 show the change of ε of SL-MM-ENMs with the content of MWCNs and GO in the electrospinning solution and the PVDF molecular weight. ε decreased as the content of nanofillers and the molecular weight of the PVDF polymer increased. This reduction is more pronounced for SL-MM-ENMs filled with GO than for MWCNs and can be related to the gradual increase of the polymer solution's surface tension, which increases bead size and density. High nanofiller concentrations also increased the electrical conductivity of the polymeric solutions,

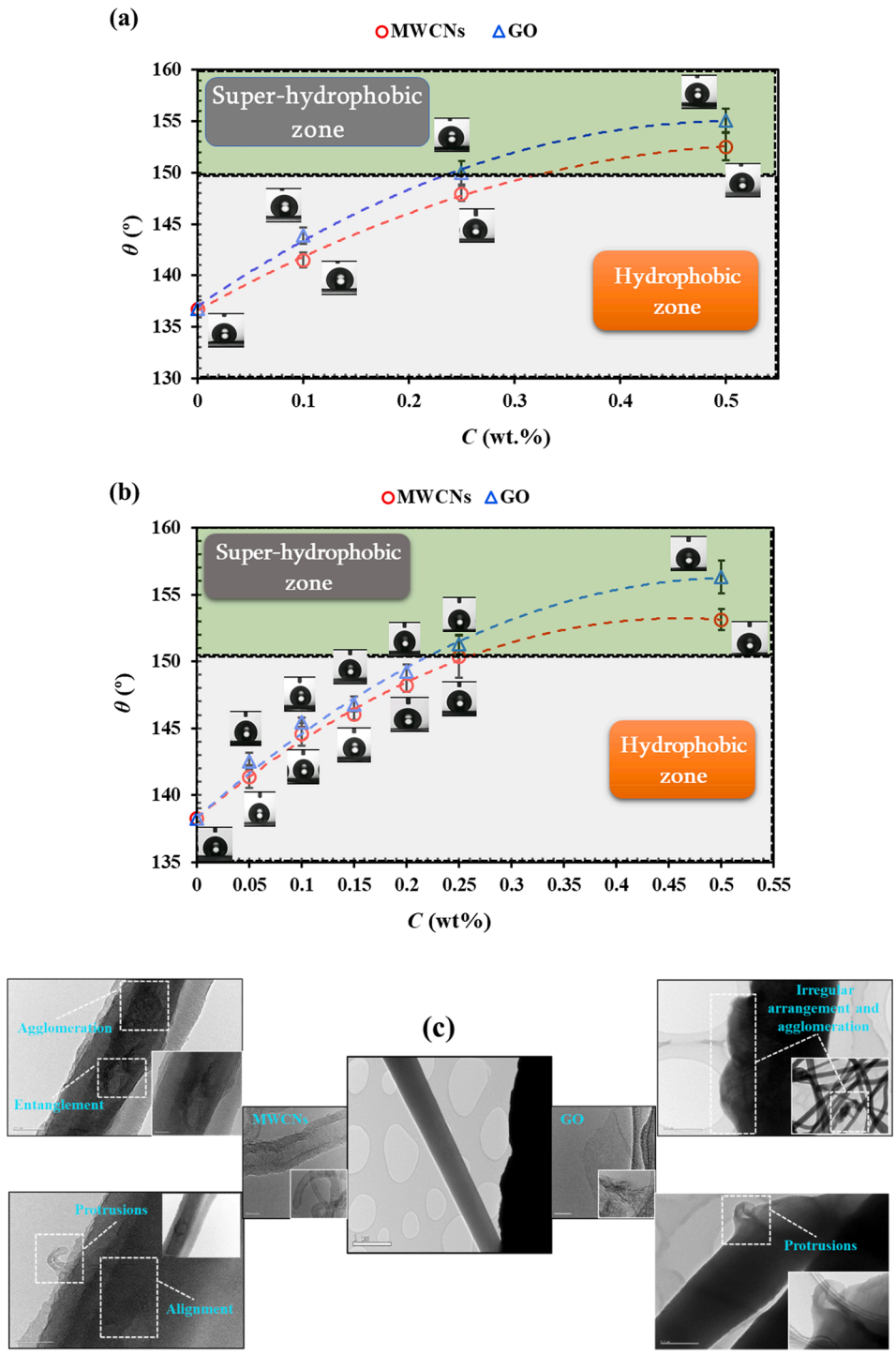

Fig. 3. Water contact angles (θ) at the surfaces of SL-MM-ENMs prepared from LMPVDF (a) and HMPVDF (b) solutions with different contents of MWCNs and GO, and TEM images showing different arrangements of MWCNs and GO in the electrospun nanofiber (c).

inducing high dissipation of electric charges to the metallic collector and less charge accumulation in the formed nanofibers. The latter effect weakens the repulsive interactions between nanofibers and thus favors more compact nanofibrous networks with low d_i and ε values. As shown in Fig. 4c, the relationship between ε and d_i was well described by a simple linear model. When the polymer solution's electrical conductivity is low, electric charges accumulate more likely within the deposited nanofibers, strengthen the repulsive interactions between them and finally result in less compact nanofibrous networks with higher d_i and ε values.

The *LEP* values determined for all SL-MM-ENMs using distilled water and a 30 g/L aqueous solution of NaCl are shown in Fig. 5. The *LEP* values for the saline solution are higher than those for distilled water due to the higher surface tension of the salt solution [51]. The observed ranges of *LEP* values are comparable to those reported for other superhydrophobic ENMs in the MD literature [14,19,39,52]. The higher *LEP* values of HMPVDF SL-MM-ENMs can be mainly attributed to their smaller maximum inter-fiber space and superhydrophobicity. Interestingly, the difference in *LEP* values between low and high molecular weight PVDF SL-MM-ENMs was more pronounced for those electrospun

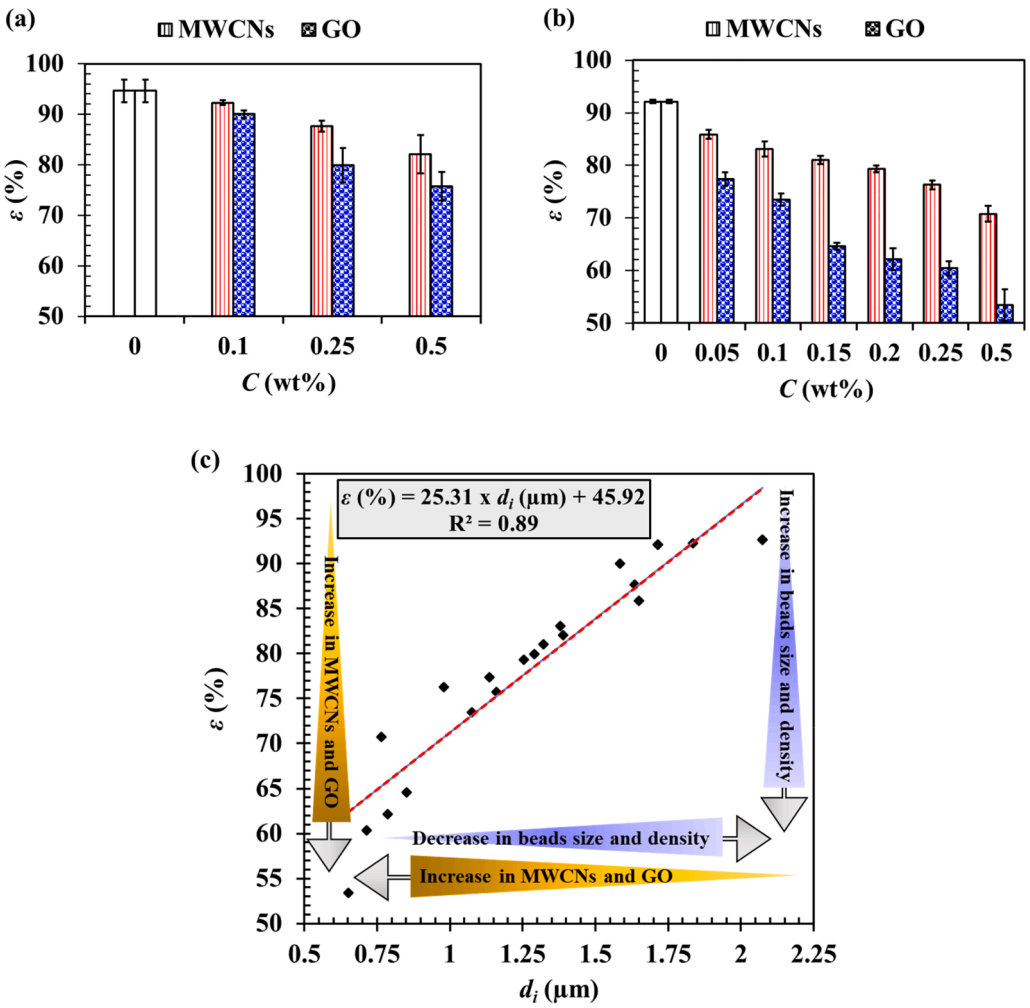

Fig. 4. Void volume fractions (ε) for LMPVDF (a) and HMPVDF (b) membranes as a function of MWCNs and GO contents, and the relationship between the void volume fraction (ε) and the inter-fiber space (d_i) (c) of SL-MM-ENMs.

with GO nanofillers than for those containing MWCNs, especially when the nanofiller concentration was high (see inset right Fig. 5a and b, Table S1, and Fig. 3a and b).

2.1.3. DCMD performance

Figs. 6 and 7 show the DCMD desalination performance of the electrospun SL-MM-ENMs. Although the pristine ENMs prepared without nanofillers (i.e. SL-0-LMPVDF and SL-0-HMPVDF) were reasonably hydrophobic ($\theta \cong 137.5°$; Fig. 3a and 3b), their DCMD permeate fluxes were higher than those of the SL-MM-ENMs. After only 2 h of operation, the electrical conductivity of the permeate of these pristine ENMs increased markedly from 4.48 µS/cm to 87.85 µS/cm for the LMPVDF membrane (Fig. 6b and d), and from 3.84 µS/cm to 2140 µS/cm for the HMPVDF membrane (Fig. 7b and d). Therefore, the pristine ENMs are unsuitable for DCMD desalination. This increase in the permeate electrical conductivity is the consequence of the low *LEP* values and the low dimensional integrity of these ENMs prepared with a short electrospinning time and without any mechanical support or heat-press post-treatment (Fig. 5a and b, and Table S1).

The salt rejection factors for all SL-MM-ENMs were above 99.99%, irrespective of the molecular weight of the used PVDF or the type of the nanofiller. For SL-MM-ENMs prepared with LMPVDF, increasing the nanofiller concentration from 0.1 wt% to 0.5 wt% reduced the permeate flux from 54.3 to 33.5 kg/m^{2}h for MWCNs and from 37.8 to 27.6 kg/m^{2}h for GO. This was attributed to the reductions of ε and d_i and the increase of δ at higher nanofiller loadings (See Fig. 4 and Table S1). For SL-MM-ENMs prepared with HMPVDF, the nanofiller content had a stronger effect on the permeate flux. Moreover, the permeate flux of HMPVDF SL-MM-ENMs containing GO was substantially lower than those of MWCNs-containing ENMs. This is attributable to their lower d_i and ε values as well as their high thickness (See Fig. 4 and Table S1).

In general, for all SL-MM-ENMs, the permeate flux decreased as the salt concentration in the aqueous feed solution was increased because of the concentration polarization effect and the reduced water vapor pressure at the feed/ENM interface (Figs. 6 and 7). Over the whole duration of the DCMD experiment (20 h), all LMPVDF and HMPVDF SL-MM-ENMs exhibited better stability than the pristine ENMs. Additionally, MWCN-containing SL-MM-ENMS with LMPVDF outperformed those containing GO. For instance, after DCMD operation, the permeate electrical conductivity of LMPVDF SL-MM-ENMs decreased from about 3.9 µS/cm to 3.0 µS/cm for the membranes prepared with MWCNs (Fig. 6b) and increased from about 3.4 µS/cm to 4.4 µS/cm for the membranes prepared with GO (Fig. 6d). For the HMPVDF SL-MM-ENMs, no clear comparison could be made for MWCNs and GO because the final electrical conductivity of both MM-ENMs decreases or increases respect to the initial permeate concentration but it was maintained below 6.1. µS/cm (Fig. 7b and 7d).

The preparation of robust MD membranes typically requires a trade-off between high permeability and excellent salt rejection. The overarching requirement is to obtain a permeate that satisfies drinking water requisites. A good membrane should exhibit the highest water production rate while satisfying this requirement. The permeate flux and its

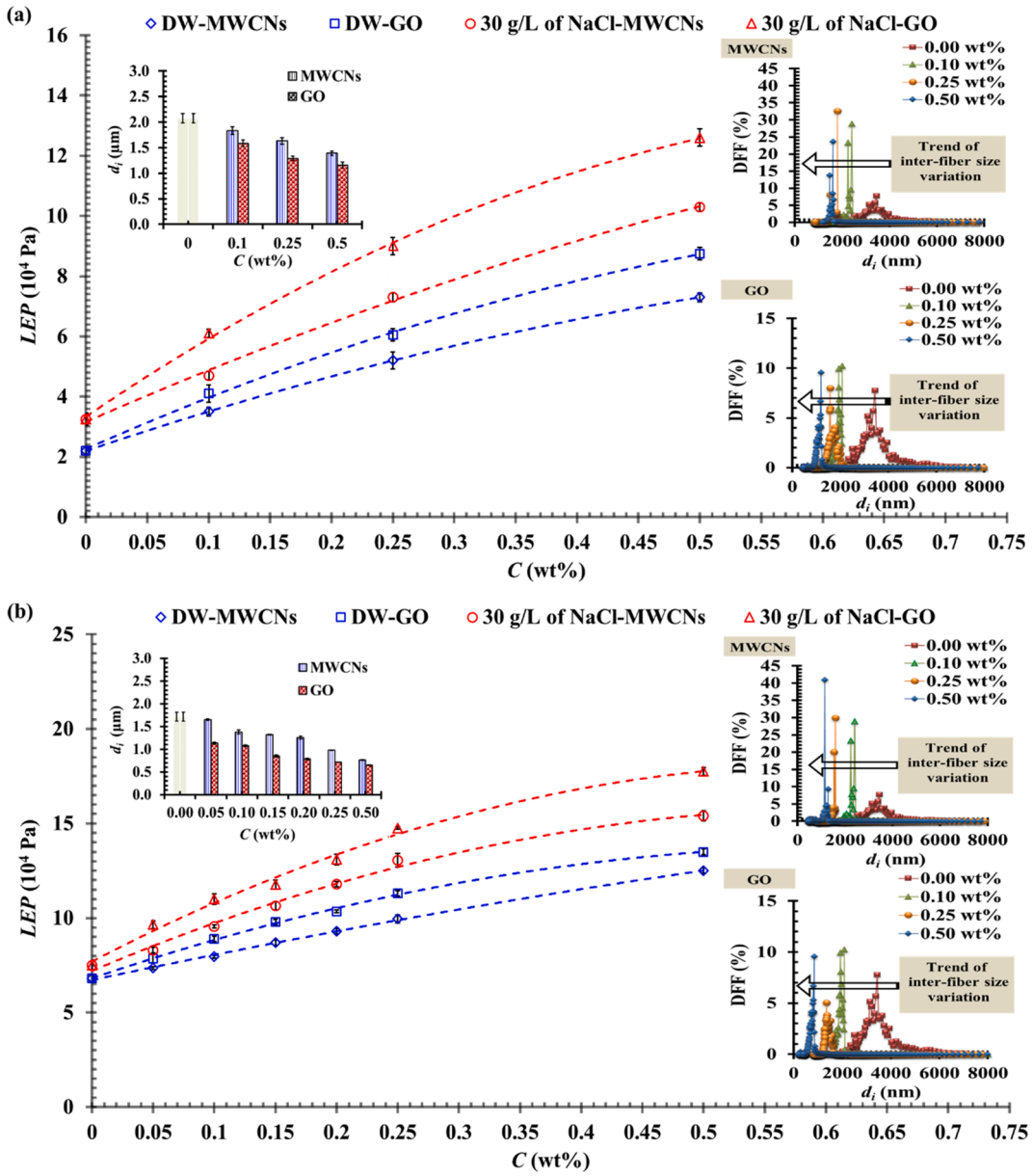

Fig. 5. Liquid Entry Pressure (*LEP*) values for distilled water and a 30 g/L NaCl aqueous solution as a function of the contents of MWCNs and GO for LMPVDF (a) and HMPVDF (b) SL-MM-ENMs. The right-hand insets show the distribution of the inter-fiber space and the left-hand insets show the variation of the mean inter-fiber space (d_i) with the nanofiller concentration.

quality can be evaluated simultaneously using the performance index (*PI*), which is defined as [53,54].

$$PI\left(\frac{kg}{m^2h}\right) = J_w\alpha \quad (1)$$

The permeate quality contribution (α) is included in the *PI* to reflect differences in DCMD performance between membranes.

Fig. S3 shows the *PI* values of the SL-MM-ENMs prepared in this work. Based on these data, the LMPVDF SL-MM-ENM prepared with 0.1 wt% MWCNs (SL-MWCNs-0.1 wt%) is the best membrane for DCMD desalination. The DCMD performance of LMPVDF SL-MM-ENMs containing 0.1 wt% nanofiller (MWCNs or GO) was superior to that reported for HMPVDF SL-MM-ENMs, especially when using MWCNs as nanofiller. Therefore, these two membranes (LMPVDF SL-MWCNs-0.1 wt% and SL-GO-0.1 wt%) were considered to be the best-performing SL-MM-ENMs and were used as the basis for the preparation of dual-layered MM-ENMs (DL-MM-ENMs) and triple-layered MM-ENMs (TL-MM-ENMs) to further improve the DCMD performance. These DL-MM-ENMs and TL-MM-ENMs were prepared using the same electrospinning procedure as the optimal SL-MM-ENMs.

2.2. Characterization and DCMD performance of DL-MM-ENMs and TL-MM-ENMs

Table 1 and Fig. 8 show the conditions used to prepare the DL- and TL-MM-ENMs and schematic depictions of their structures.

2.2.1. Morphological structure

Fig. 9 shows FESEM images of the surfaces of some DL-MM-ENMs and TL-MM-ENMs prepared with the same total electrospinning time (90 min). The bottom layers' surface morphology is characterized by multiple beads, hills, and agglomerated groups of nanofibers. These structural features favor the formation of tightly adherent composite nanofibrous structures with bonded beads and welded fibers, especially

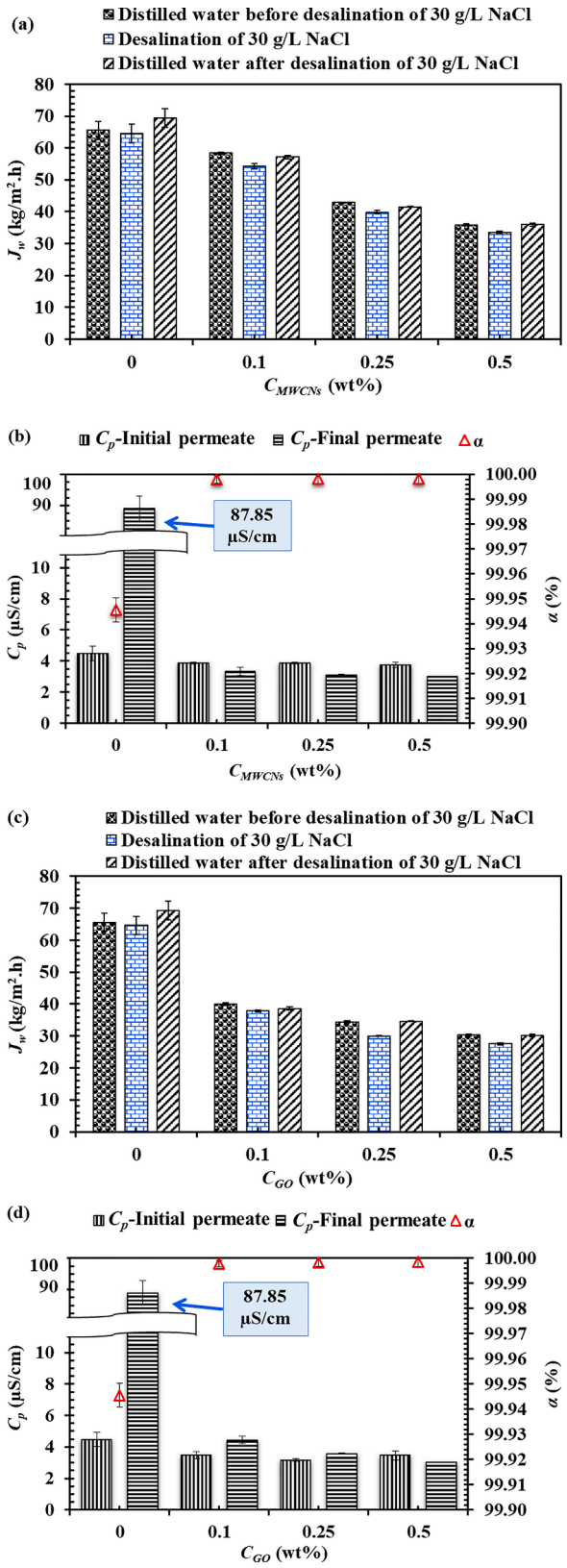

Fig. 6. (a) and (c) Permeate flux (J_w); (b) and (d) salt rejection factor (α), together with initial and final electrical conductivity (χ_p) of the permeate for LMPVDF-ENMs, as a function of the concentrations of MWCNs and GO, respectively using distilled water and 30 g/L NaCl aqueous feed solutions. Feed temperature (T_f) = 80°C, permeate temperature (T_p) = 20°C, stirring rate (w) = 500 rpm.

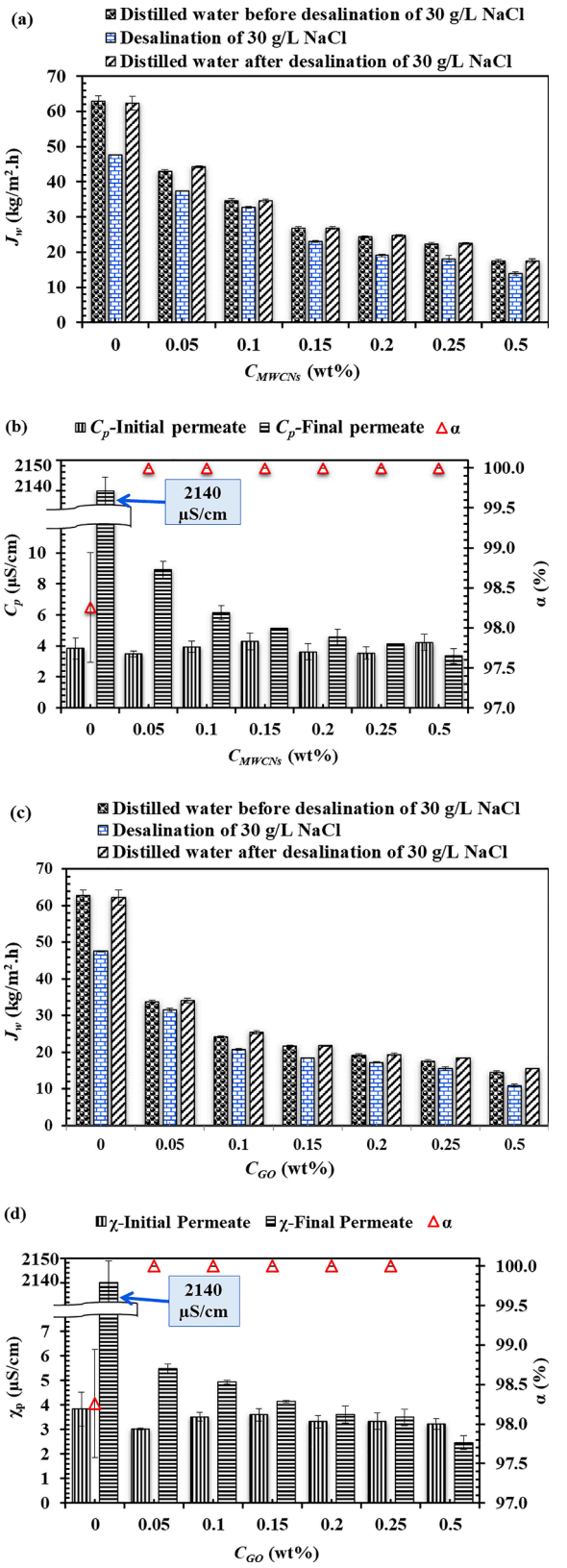

Fig. 7. (a) and (c) Permeate flux (J_w); (b) and (d) salt rejection factor (α); and the initial and final electrical conductivity (χ_p) of the permeates for HMPVDF ENMs as a function of their MWCNs and GO contents, respectively, using distilled water and 30 g/L NaCl aqueous feed solutions. Feed temperature (T_f) = 80°C, permeate temperature (T_p) = 20°C, stirring rate (w) = 500 rpm.

Table 1
Polymer solutions and electrospinning time (t_e) for the preparation of DL-MM-ENMs and TL-MM-ENMs layers.

ENMs code	Bottom layer		Middle layer		Top layer		Total time
	t_e (min)	type	t_e (min)	type	type	t_e (min)	
SL-0-LMPVDF	60	LMPVDF	–		–	0	60
SL-MWCNs-0.1 wt%	60	MWCNs-LMPVDF	–		–	0	60
DL-1	30	MWCNs-LMPVDF	–		PSF	30	60
DL-2	30	MWCNs-LMPVDF	–		PSF	60	90
DL-3	30	MWCNs-LMPVDF	–		LMPVDF	60	90
DL-4	45	MWCNs-LMPVDF	–		PSF	45	90
SL-GO-0.1 wt%	60	GO-LMPVDF	–		–	0	60
DL-5	30	GO-LMPVDF	–		PSF	30	60
DL-6	30	GO-LMPVDF	–		PSF	60	90
DL-7	30	GO-LMPVDF	–		LMPVDF	60	90
DL-8	45	GO-LMPVDF	–		PSF	45	90
TL-9	30	MWCNs-LMPVDF	30	PSF	MWCNs-LMPVDF	30	90
TL-10	30	MWCNs-LMPVDF	30	LMPVDF	MWCNs-LMPVDF	30	90
TL-11	30	GO-LMPVDF	30	PSF	GO-LMPVDF	30	90
TL-12	30	GO-LMPVDF	30	LMPVDF	GO-LMPVDF	30	90

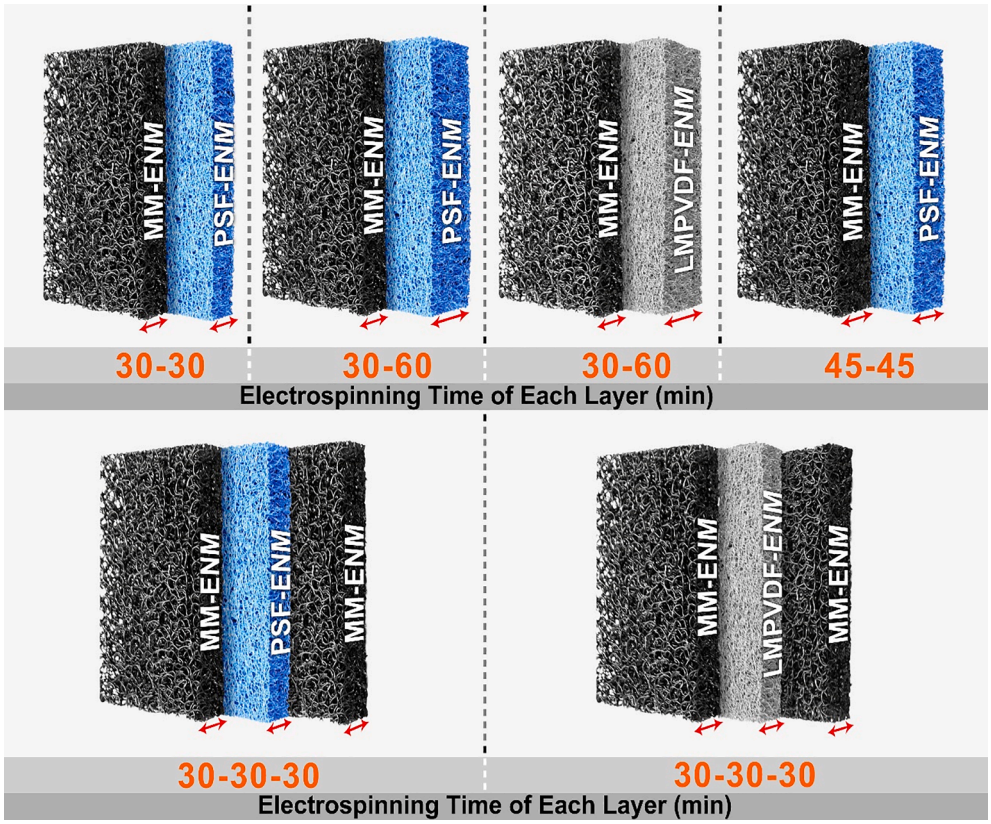

Fig. 8. Schematic depictions of the dual and triple-layered MM-ENMs.

when the layer deposited on the top is LMPVDF (as in DL-3 and DL-7). The electrical conductivity of the LMPVDF polymer solution loaded with MWCNs or GO is considerably higher than that of LMPVDF, resulting in better dissipation of electrical charges to the metal collector through the bottom layer. Consequently, the charge accumulation in the nascent LMPVDF nanofibers is low, which weakens the repulsive interactions between fibers and results in a compact top nanofibrous network with low inter-fiber space. The compactness of the top layer (LMPVDF-ENM) slows the evaporation of the solvent from the bottom layer, but also promotes welding of the two layers and the formation of strong attractive interactions between nanofibers. These phenomena are less pronounced for DL-MM-ENMs containing PSF-ENM as a top layer because of the looser structure of PSF layer (i.e. higher void volume fraction), which enables rapid solvent evaporation from the bottom layer and therefore yields a nanofibrous structure with fewer welds.

2.2.2. Thickness, void volume fraction, liquid entry pressure, contact angle, and inter-fiber space

The thickness (δ), void volume fraction (ε), liquid entry pressure (*LEP*), and contact angles (θ) of the prepared DL-MM-ENMs and TL- MM-ENMs are shown in Figs. S4 and S5, and summarized in Table S2. As it was expected, the total thickness of the DL-MM-ENMs increased as the electrospinning time of the PSF polymer solution was increased (see Fig. S4a). Although the total electrospinning time of the DL-MM-ENMs (DL-2, DL-3, DL-6, and DL-7) was kept at 90 min, the total thickness decreased when the PSF layer was replaced by the LMPVDF layer (Fig. S4a, DL-2 vs. DL-3 and DL-6 vs. DL7). This can be attributed to the greater compaction of the nanofibrous network of the LMPVDF layer

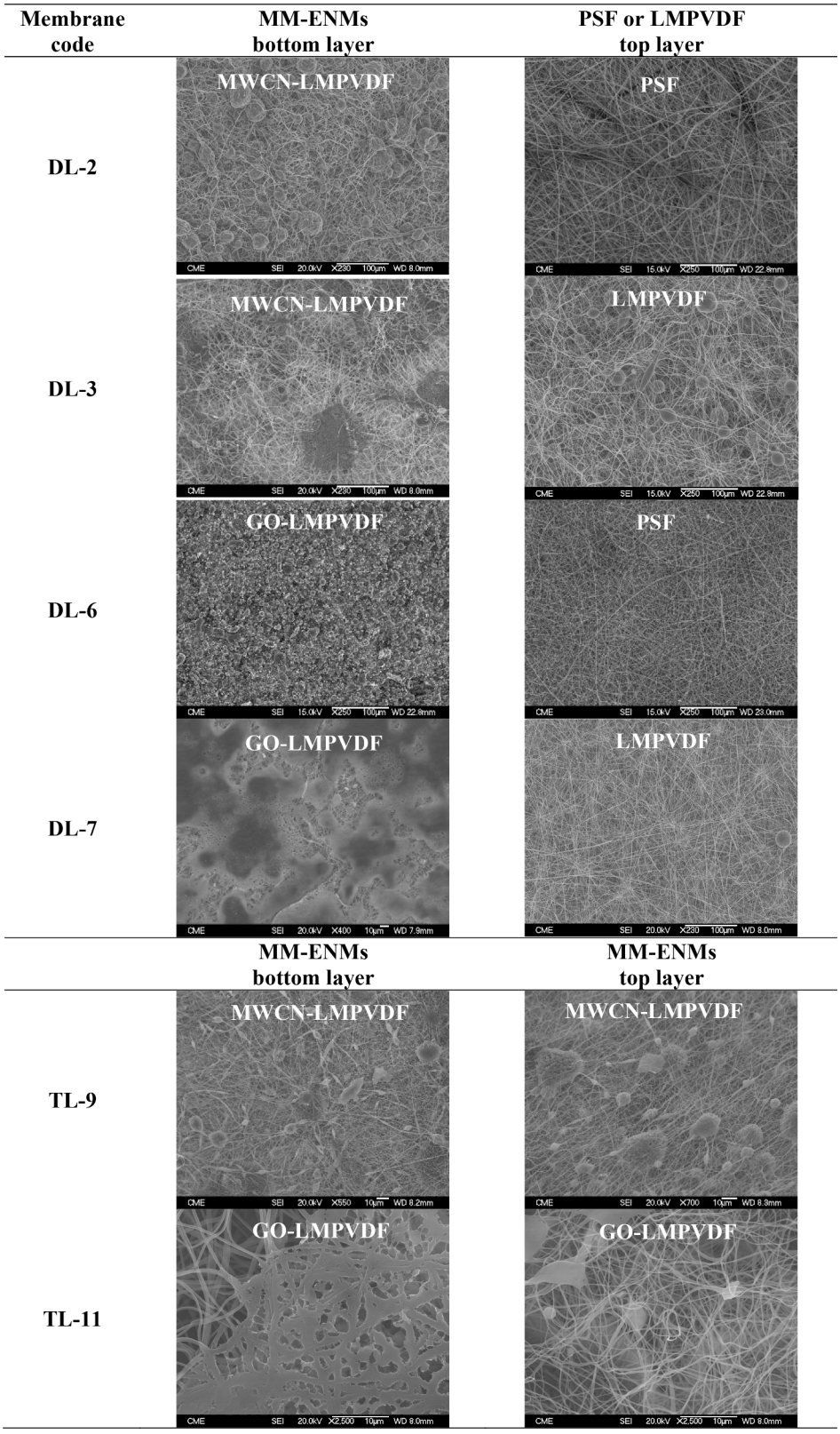

Fig. 9. FESEM images of DL-MM-ENMs and TL-MM-ENMs.

compared to the PSF layer. The thickness of the TL-MM-ENMs did not vary significantly and it was maintained generally around 706.4 μm, (Fig. S4c).

The overall ε values of the DL-MM-ENMs are presented in Fig. S4.a. These depend on both ε and δ of each layer (i.e. electrospinning time) and the nature of the top layer (PSF or LMPVDF). Increasing the PSF layer's electrospinning time from 30 to 60 min caused an increase of ε (compare DL-1 to DL-2 and DL-5 to DL-6). Conversely, when the PSF layer was replaced by LMPVDF, ε declined (compare DL-2 to DL-3 and DL-6 to DL-7). In addition, ε also decreased as δ of the MM-ENM layer

was increased (compare DL-1 to DL-4 and DL-5 to DL-8). The ε values of the TL-MM-ENMs decreased when the interlayer was changed from PSF to LMPVDF and when GO was used as nanofiller rather than MWCNs (Fig. S4b).

The inter-fiber space (mean, minimum, and maximum) and its distribution in the DL-MM-ENMs (DL-2, DL-3, DL-6, and DL-7) and TL-MM-ENMs (TL-9, TL-10, TL-11, and TL-12) prepared with a total electrospinning time of 90 min are shown in Fig. 10. The inter-fiber size distribution curves of the DL-MM-ENMs and TL-MM-ENMs shifted towards smaller values when the PSF layer was replaced by the LMPVDF layer. For both DL-MM-ENMs and TL-MM-ENMs, smaller inter-fiber spaces were obtained with GO nanofiller than with MWCNs, regardless of the choice of the middle layer polymer (Fig. 10a and b). This was due to the extra compaction of the nanofibrous network in DL-MM-ENMs and TL-MM-ENMs caused by the LMPVDF layer and the increased agglomeration welding of nanofiber webs when using GO as nanofiller rather than MWCNs (see Fig. 9). The maximum, mean, and minimum inter-fiber spaces of the electrospun MM-ENMs are shown in Fig. 10c. The inter-fiber space decreased upon replacing the PSF layer with LMPVDF and when changing the MWCNs nanofiller by GO. The reasons for these trends are similar to those discussed previously in relation to the void volume fraction (Fig. S4). These two effects reduced the maximum inter-fiber space by more than two-fold affecting considerably the *LEP*.

The measured *LEP* values of all DL-ENMs and TL- MM-ENMs for distilled water and 30 g/L aqueous solutions of NaCl are presented in Fig. S5 and Table S2. The *LEP* values of TL-MM-ENMs were higher than those of DL-MM-ENMs, especially for the 30 g/L NaCl aqueous solution. This was partly due to the reduction of the maximum inter-fiber space, as shown in Fig. 10c.

The θ values of the first (bottom) layer deposited on the metallic collector during electrospinning are presented in Table S2 and Fig. S5 for all DL-MM-ENMs and TL-MM-ENMs. In DCMD, the bottom layer was brought in direct contact with the hot feed solution. The DL-MM-ENMs (i.e. DL-5, DL-6, DL-7, and DL-8) and TL-MM-ENMs (i.e. TL-11 and TL-12) filled with GO had higher θ values than those filled with MWCNs (DL-1, DL-2, DL-3, and DL-4, TL-9 and TL-10 respectively). This observation was discussed in Section 2.2.1. It was also observed that electrospinning of the second layer (i.e. the top layer in DL-MM-ENMs) and the other layers in TL-MM-ENMs had no appreciable effect on the θ values of the bottom layer.

2.2.3. Mechanical properties

The stress–strain curves of the pristine SL-0-LMPVDF membrane and the DL-MM-ENMs are presented in Fig. 11. The tensile strength (T_S) and elongation at break (E_b) values of these ENMs are listed in Table S3. All DL-MM-ENMs had an echelon corresponding to the rupture of the hydrophilic PSF layer before that of the hydrophobic layer. This was confirmed by visual inspection while characterizing the samples' mechanical properties. For DL-3 and DL-7, which have an upper layer of LMPVDF, the bottom layer containing the nanofillers (MWCNs or GO) broke before the upper nanofiller-free LMPVDF layer. This echelon was not observed for pristine SL (i.e. SL-0-LMPVDF) or SL-MM-ENMs (i.e. SL-MWCNs-0.1 wt% and SL-GO-0.1 wt%). Therefore, the strain-deformation and the deformation at the point of rupture of the hydrophilic (PSF) and hydrophobic (LMPVDF) layers of the DL-MM-ENMs (i.e. DL-1, DL-2, DL-4, DL-5, DL-6, and DL-8) were determined from the first observed echelon. Conversely, the corresponding values of the mixed matrix LMPVDF bottom layer of the DL-MM-ENMs (i.e. DL-3 and DL-7) were determined from the end point of the strain-deformation curve (i.e. the breaking point). The tensile strength (*Ts*) and elongation at break (E_b) of the DL-MM-ENMs increased slightly with the increase of the electrospinning time from 30 to 60 min and with the increase of the PSF

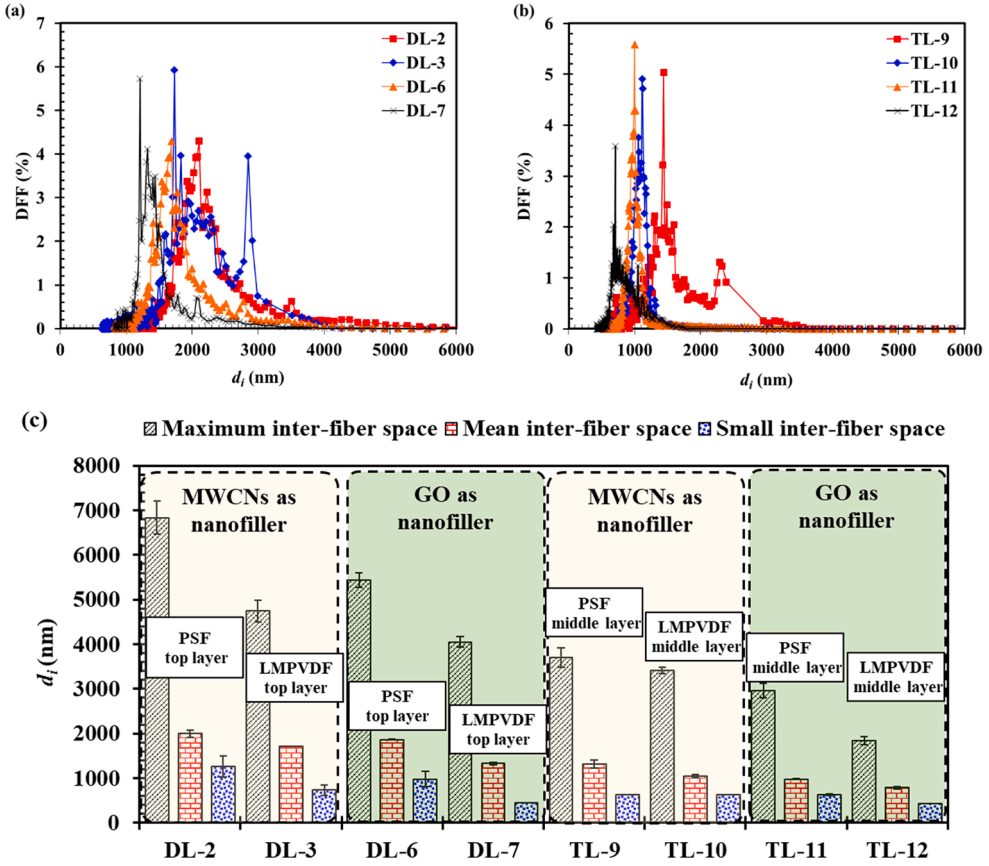

Fig. 10. Inter-fiber space (d_i) distributions of DL-MM-ENMs (a) and TL-MM-ENMs (b) prepared with the same electrospinning time (90 min), and the maximum, mean and minimum inter-fiber spaces of DL-MM-ENMs and TL-MM-ENMs (c).

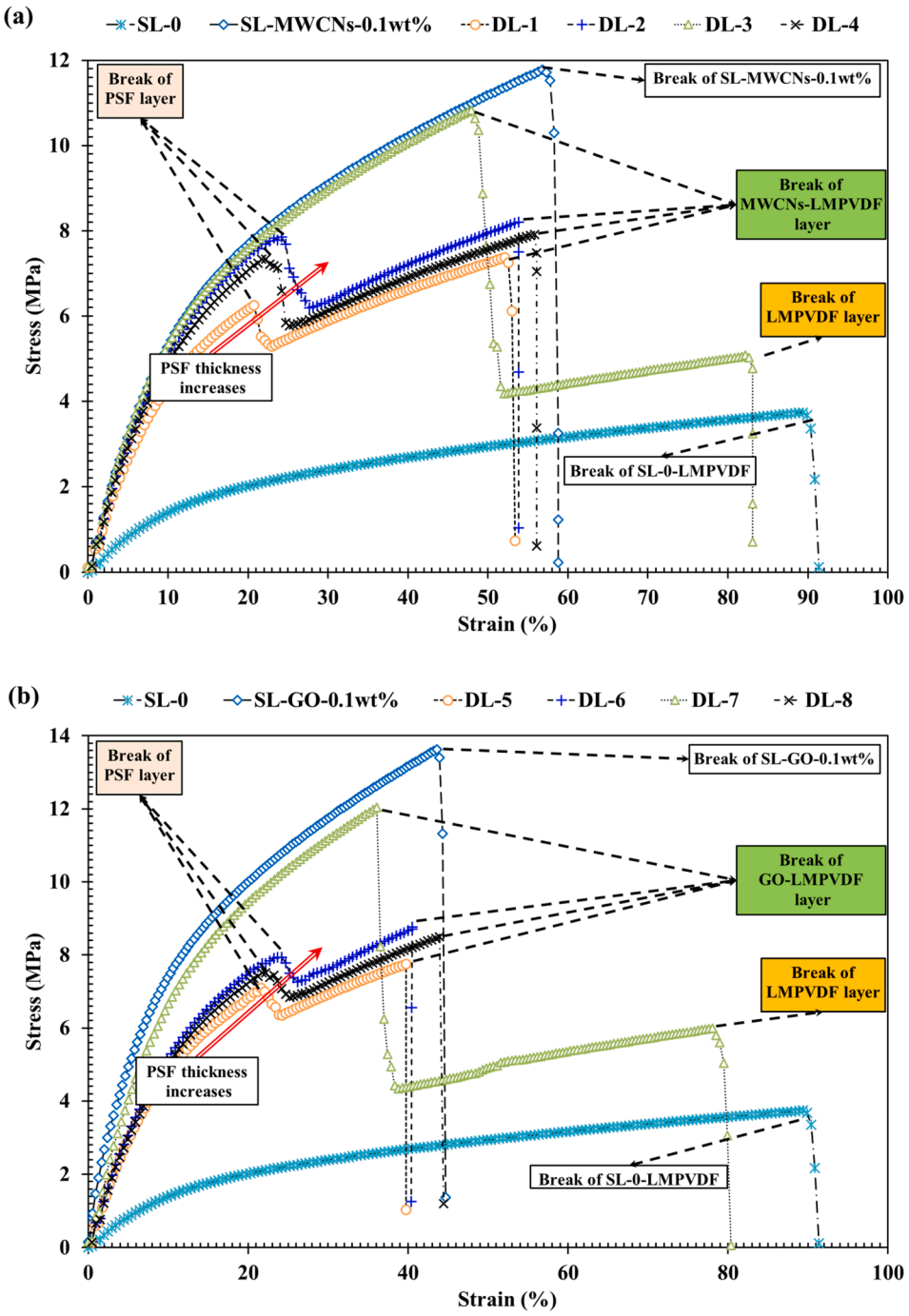

Fig. 11. Stress–strain curves of the SL-ENM, SL-MM-ENM, and DL-MM-ENMs prepared with LMPVDF and two different nanofillers: MWCNs (a) and GO (b).

layer's thickness. This trend can be attributed to the increase of the total thickness of the DL-MM-ENMs. The tensile strength (T_S) and the elongation at break (E_b) of DL-3 (i.e. MW-LMPVDF/LMPVDF) are 1.4 and 1.5 times greater than those of DL-2 (i.e. MW-LMPVDF/PSF), respectively; while those of DL-7 (i.e. GO-LMPVDF/LMPVDF) are 1.5 and 2.1 times greater than those of DL-6 (i.e. GO-LMPVDF/PSF), respectively.

Fig. 12 shows the tensile stress-strain behavior of TL-MM-ENMs and DL-MM-ENMs prepared with a total electrospinning time of 90 min. For all TL-MM-ENMs there is an echelon corresponding to the simultaneous rupture of the top and bottom layers prior to the rupture of the middle layer (PSF or LMPVDF). This behavior was confirmed by visual inspection during the characterization of the samples' mechanical properties. The TL-MM-ENMs exhibited better tensile strengths than the DL-MM-ENMs, and the difference was more pronounced for TL-MM-ENMs with GO-filled bottom and top layers than for those filled with MWCNs, especially in TL-MM-ENMs electrospun with LMPVDF middle layer. Therefore, both the nanofiller type and the nature of the middle layer affect the mechanical properties of TL-MM-ENMs.

2.2.4. DCMD performance

Fig. 13 shows the DCMD permeate fluxes (J_w) of DL-MM-ENMs using 30 g/L aqueous solution of NaCl as feed. The permeate flux was also measured using distilled water as feed before and after DCMD desalination. In these experiments, the bottom mixed matrix layer (i.e. first electrospun layer) was brought into contact with the feed solution. The DL-2 and DL-6 membranes exhibited higher permeate fluxes than those

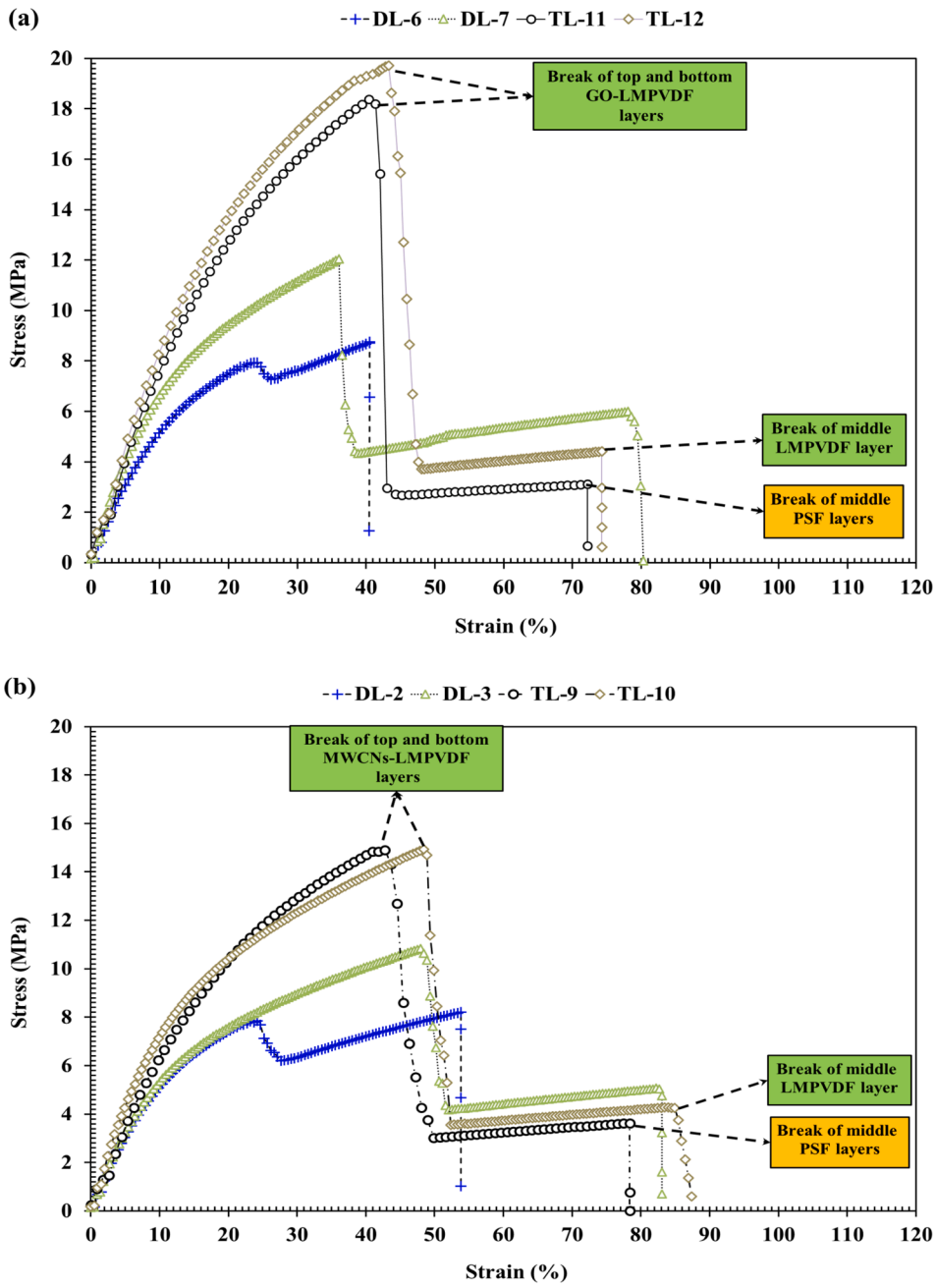

Fig. 12. Stress–strain curves of TL-MM-ENMs and DL-MM-ENM prepared with different nanofillers: GO (a) and MWCNs (b).

of the pristine SL-0-LMPVDF and SL-MM-ENMs (SL-MWCNs-0.1 wt% and SL-GO-0.1 wt%) prepared with LMPVDF. It was also observed a clear enhancement of the permeate flux of the DL-MM-ENMs prepared with MWCNs and GO with the increase of the thickness of the PSF hydrophilic layer (i.e. the electrospinning time of the PSF hydrophilic layer was increased from 30 to 60 min) as can be seen when comparing DL-1 with DL-2 and DL-5 with DL-6. This was attributed to the increase of the void volume fraction as the PSF polymer solution's electrospinning time was increased (Fig. S4a and Table S2) and the possible reduction of the heat transfer by conduction through the whole DL-MM-ENMs. In previous studies it was claimed that hydrophobic/hydrophilic composite membranes could achieve high permeate fluxes in MD by combining a thin hydrophobic layer with a thicker hydrophilic layer [23,32]. The thin hydrophobic porous layer was proposed to reduce the resistance to vapor diffusion, while the thicker hydrophilic layer with bigger pores was considered to reduce the path length of water vapor transport, allowing faster permeation, and lower heat loss by conduction increasing therefore the thermal efficiency of the DCMD process [25]. It claimed that the increase of the thermal conductivity of the hydrophilic layer of composite hydrophobic/hydrophilic membranes improved the DCMD permeate flux reaching asymptotic value because of the increase of the temperature polarization coefficient [50].

From the comparison of DL-2 with DL-4 and DL-6 with DL-8 ENMs, it can be stated that the permeate flux declined with the increase of the thickness of the hydrophobic layer (i.e. electrospinning time from 30 min to 45 min) and the decrease of the electrospinning time of the hydrophilic layer from 60 min to 45 min. This result is attributed to the reduction of the void volume fraction as the electrospinning time of the LMPVDF-MWCNS polymer solution was increased (Fig. S4a and Table S2). In fact, the presence of a thick hydrophobic porous layer increases the vapor diffusion resistance [25].

For the same electrospinning conditions, when the hydrophilic layer

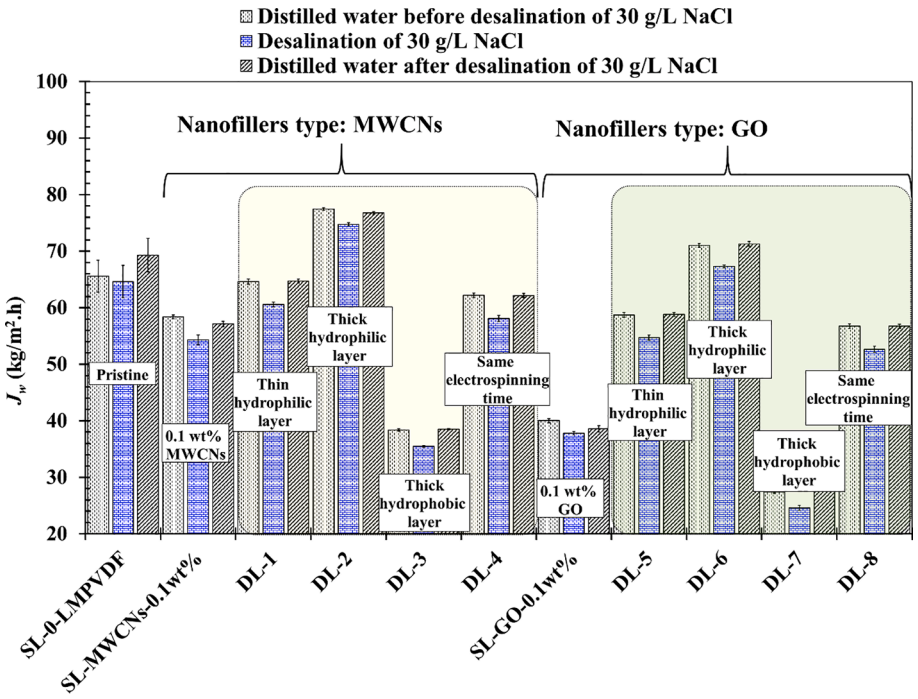

Fig. 13. DCMD permeate flux (J_w) of the DL-MM-ENMs together with those of the SL-MM-ENMs (SL-MWCN-0.1 wt% and SL-GO-0.1 wt%) and pristine SL-ENM (SL-0-LMPVDF). The feed solutions were distilled water and 30 g/L NaCl aqueous solution with a feed temperature (T_f) of 80°C, a permeate temperature (T_p) of 20°C and a stirring rate (w) of 500 rpm.

was replaced with the hydrophobic one (compare DL-2 with DL-3 and DL-6 with DL-7), the DCMD permeate flux was reduced. This decrease was more pronounced when using GO as nanofiller rather than MWCNs. This result is due to the decrease of the void volume fraction (Fig. S4a and Table S2) and to the higher resistance to mass transfer for water vapor diffusion through the DL-MM-ENMs electrospun with different hydrophobic layers (DL-3 and DL-7) compared to the hydrophobic/hydrophilic MM-ENMs (DL-2 and DL-6). In other words, the hydrophilic layer's greater propensity for wetting of the inter-fiber space (when compared to hydrophobic layer) may facilitate water penetration into the membrane structure from the permeate side and thereby reduce the distance between the liquid/vapor interfaces formed on each side of the hydrophobic layer, leading to a higher permeate flux. This improvement should become more pronounced for membranes with thinner hydrophobic layer and/or thicker hydrophilic layer.

In general, all DL-MM-ENMs exhibited high salt rejection factors (>99.99%). The final electrical conductivity of the permeate was 8.38 ± 4.66 μS/cm and 6.57 ± 4.43 μS/cm for the DL-MM-ENMs prepared with MWCNs and GO, respectively. For comparative purposes, the salt rejection factor of the pristine SL-ENM (SL-0-LMPVDF) was 99.94% and its permeate electrical conductivity increased from 4.48 to 87.85 μS/cm during the first 2 h of DCMD operation with a feed solution containing 30 g/L NaCl. The superior performance of the DL-MM-ENMs was attributed to their higher *LEP* values and smaller maximum inter-fiber spaces (Fig. S5a and Table S2). The final electrical conductivity of the SL-MM-ENMs prepared with MWCNs (SL-MWCNs-0.1 wt%) and GO (SL-GO-0.1 wt%) were 3.36 μS/cm and 4.44 μS/cm, respectively.

The membrane DL-2 was found to be the most promising DL-MM-ENMs for DCMD desalination as it achieved a salt rejection factor of 99.995% (i.e. a final permeate electrical conductivity of 7.629 μS/cm) with a high permeate flux of 74.75 kg/m^{2}h. These values compare favorably to those reported for the CENM–5 PVDF/PSF membrane prepared with an electrospinning time of 0.5 h for the PVDF layer and 2.5 h for the PSF layer [23]. The reported permeate flux of this membranes was 47.7 kg/m^{2}h with a salt rejection factor of 99.99% when using a 30 g/L aqueous NaCl feed solution with a temperature difference of 60°C. The DCMD performance of the membrane DL-2 is also higher than that of a dual-layer bicomponent nanofibrous composite membrane proposed by Leonard et al. [25] using poly (vinylidene fluoride-co-hexafluoropropylene) (PVDF-HFP) nanofiberous layer and polyacrylonitrile (PAN) microfibrous layer (PVDF-HFP/PAN). The reported permeate flux of this membrane was 30 kg/m^{2}h with a salt rejection factor above 99% when using 35 g/L NaCl aqueous solution as feed with a temperature difference of 40°C. Zhao et al. [29] prepared activated carbon (AC) hydrophobic/hydrophilic dual-layer nanofibrous composite membranes using PVDF-HFP as the hydrophobic layer and the commercial Biodyne-A Nylon 6,6 as the hydrophilic layer. This membrane achieved a permeate flux of 45.6 kg/m^{2}h with a salt rejection factor of 99.95% when using 35 g/L NaCl aqueous feed solution with a temperature difference of 45°C.

Fig. 14 shows the DCMD permeate fluxes (J_w) of the TL-MM-ENMs using as feed 30 g/L NaCl aqueous solution and distilled water before and after DCMD desalination experiment. Among the TL-MM-ENMs, the lowest obtained permeate flux was around 33.6 kg/m^{2}h for the membrane TL-12 (GO/LMPVDF/GO), while the highest one was 56.6 kg/m^{2}h for the membrane TL-9 (MWCNs/PSF/MWCNs). In general, the permeate fluxes of the TL-MM-ENMs were mostly lower than those of the DL-MM-ENMs. It was also observed a decline of the permeate flux upon changing the interlayer from PSF to LMPVDF and when replacing the nanofiller from MWCNs to GO. These results are attributed to the reduction of the void volume fraction (Table S2 and Fig. S4b), the compacted LMPVDF layer in the nanofibrous network of the TL-MM-ENMs and the increased nanofiber agglomeration and network welding caused by changing the nanofiller from MWCNs to GO.

The salt rejection factor of all TL-MM-ENMs were above 99.98%. The final permeate electrical conductivity of the membrane TL-10, 3.923 μS/cm, was almost identical to the initial value, 3.813 S/cm. However, for the membrane TL-12 the final permeate electrical conductivity, 2.015 μS/cm was appreciably lower than the initial value, 3.699 μS/cm. This is due to the higher *LEP* values (Fig. S5) and the lowest maximum inter-fiber space of the TL-12 (i.e. $d_{i,\max}$ = 1845 ± 92 nm) membrane compared to those of the TL-10 membrane (i.e. $d_{i,\max}$ = 3410 ± 71 nm),

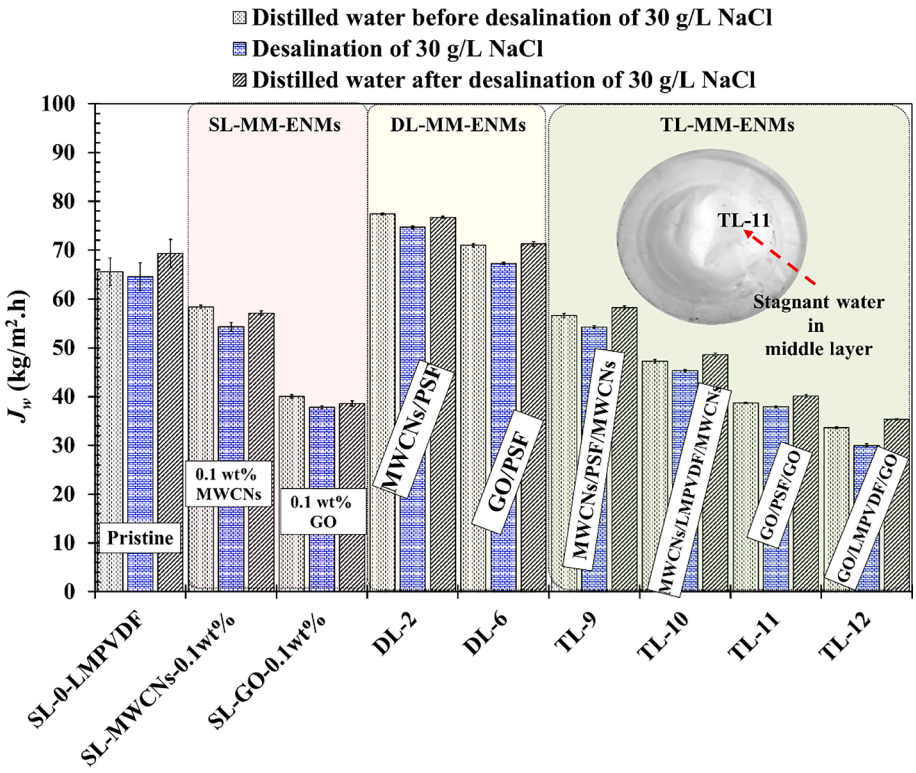

Fig. 14. Permeate fluxes (J_w) of the TL-MM-ENMs together with those of the DL-MM-ENMs (DL-2 and DL-6), SL-MM-ENMs (SL-MWCN-0.1 wt% and SL-GO-0.1 wt%) and pristine SL-ENM (SL-0-LMPVDF). The feed solutions were distilled water and 30 g/L NaCl aqueous solution with a feed temperature (T_f) of 80°C, a permeate temperature (T_p) of 20°C and a stirring rate (w) of 500 rpm.

see Fig. 10.

Unexpectedly, sandwiching a hydrophilic layer between two hydrophobic layers (TL-9 and TL-11) resulted in an increased final permeate electrical conductivity, to 10.49 μS/cm and 19.10 μS/cm, respectively; in DCMD experiments where the initial permeate electrical conductivity was 3.63 μS/cm. This was due to the formation of water pockets within these membranes observed after DCMD experiments as shown in Fig. 14. This can be associated to the condensation of water vapor in the membrane's hydrophilic layer. To test this hypothesis, both TL-MM-ENMs were opened after the DCMD experiments and effectively trapped stagnant water in the hydrophilic layer of these membranes was detected. We therefore concluded that DCMD membrane design should not consider any internal hydrophilic layer sandwiched between two hydrophobic layers provided that it promotes water condensation.

3. Conclusions

MM-ENMs with favorable mechanical and hydrophobic properties for DCMD were electrospun by mixing nanofillers (MWCNs or GO) with polymeric solutions of different PVDF molecular weights, LMPVDF and HMPVDF. Using analytical techniques, it was shown that high nanofiller concentrations promoted bead formation in single-layer MM-ENMs. As a result, a superhydrophobic character was observed in SL-MM-ENMs prepared from LMPVDF and HMPVDF with both GO and MWCNs contents above 0.25 wt%. A higher nanofiller concentration (i.e. 0.5 wt% of MWCNs or GO) induced smaller inter-fiber space of SL-MM-ENMs prepared with LMPVDF by 33.17% and 44.22% while those prepared with HMPVDF by 55.23% and 62.21% when using MWCNs and GO, respectively. This favored the improvement of the liquid entry pressure, by 3.32 and 3.97 times for LMPVDF ENMs, and 1.84 times and 1.99 times for HMPVDF ENMs, when using MWCNS and GO, respectively.

The SL-MM-ENMs prepared from LMPVDF and 0.1 wt% nanofiller, either MWCNs or GO, exhibited good DCMD desalination performance. Particularly, the SL-MM-ENMs prepared with LMPVDF and 0.1 wt% MWCNs (SL-MWCNs-0.1 wt%) exhibited good surface hydrophobicity, with a water contact angle near 142°, a high permeate flux (~54 kg/m^{2}h), an excellent salt rejection factor (~99.99%), without wetting the inter-fiber space during a 10 h DCMD experiment.

Better DCMD performance was achieved using dual-layered MM-ENM (DL-2) with permeate fluxes of 77.5, 74.7, and 76.7 kg/m^2·h and salt (NaCl) rejection factors up to 99.995% in sequential DCMD experiments using as feed distilled water, 30 g/L NaCl aqueous solution and distilled water, respectively, being the feed temperature 80°C and the permeate temperature 20°C. The electrical conductivity of the permeate remained stable at around 7.63 ± 0.49 μS/cm during a 10 h DCMD experiment, starting from an initial value of 4.89 ± 0.76 μS/cm.

Although the mechanical properties of the triple-layered membranes (TL-MM-ENMs) and their *LEP* values were significantly better than those of the DL-MM-ENMs, their permeate fluxes were considerably lower especially if the middle layer is made of LMPVDF and the nanofiller is GO. The electrospun TL-MM-ENMs with an internal hydrophilic layer sandwiched between two hydrophobic layers exhibited substantial water condensation (i.e. water pocket formation) during DCMD experiments. Such an engineered membrane design is not suitable for DCMD.

It was found that integrating MWCNs into the active surface of DL-MM-ENMs is an attractive strategy for preparing membranes with superior DCMD desalination performance.

Declaration of Competing Interest

The authors declare that they have no known competing financial interests or personal relationships that could have appeared to influence the work reported in this paper.

Acknowledgments

We appreciate the financial support from the Kempe Foundation and the Bio4energy program, the Spanish Ministry of Economy and

Competitiveness through its project No. CTM2015-65348-C2-2-R and the Spanish Ministry of Science, Innovation and Universities through its project No. RTI2018-096042-B-C22.

Appendix A. Supplementary data

Supplementary data to this article can be found online at https://doi.org/10.1016/j.cej.2021.131316.

References

[1] M. Khayet, T. Matsuura, Membrane distillation: principles and applications, Elsevier, 2011.
[2] A. Alkhudhiri, N. Darwish, N. Hilal, Membrane distillation: A comprehensive review, Desalination 287 (2012) 2–18.
[3] A. Deshmukh, M. Elimelech, Understanding the impact of membrane properties and transport phenomena on the energetic performance of membrane distillation desalination, J. Membr. Sci. 539 (2017) 458–474.
[4] T. Zhou, Y. Yao, R. Xiang, Y. Wu, Formation and characterization of polytetrafluoroethylene nanofiber membranes for vacuum membrane distillation, J. Membr. Sci. 453 (2014) 402–408.
[5] H. Xu, W. Jin, F. Wang, G. Liu, C. Li, J. Wang, H. Zhu, Y. Guo, Formation and characterization of polytetrafluoroethylene nanofiber membranes for high-efficiency fine particulate filtration, RSC Advances 9 (24) (2019) 13631–13645.
[6] B.S. Lalia, E. Guillen-Burrieza, H.A. Arafat, R. Hashaikeh, Fabrication and characterization of polyvinylidenefluoride-co-hexafluoropropylene (PVDF-HFP) electrospun membranes for direct contact membrane distillation, J. Membr. Sci. 428 (2013) 104–115.
[7] Y. Zhang, B. Yang, K. Li, D. Hou, C. Zhao, J. Wang, Electrospun porous poly (tetrafluoroethylene-co-hexafluoropropylene-co-vinylidene fluoride) membranes for membrane distillation, RSC Advances 7 (89) (2017) 56183–56193.
[8] J.A. Prince, D. Rana, G. Singh, T. Matsuura, T. Jun Kai, T.S. Shanmugasundaram, Effect of hydrophobic surface modifying macromolecules on differently produced PVDF membranes for direct contact membrane distillation, Chem. Eng. J. 242 (2014) 387–396.
[9] C. Ursino, E. Di Nicolò, B. Gabriele, A. Criscuoli, A. Figoli, Development of a novel perfluoropolyether (PFPE) hydrophobic/hydrophilic coated membranes for water treatment, Journal of Membrane Science 581 (2019) 58–71.
[10] B. Li, Y. Cui, T.-S. Chung, Hydrophobic perfluoropolyether-coated thin-film composite membranes for organic solvent nanofiltration, ACS Applied Polymer Materials 1 (3) (2019) 472–481.
[11] R. Zheng, Y. Chen, J. Wang, J. Song, X.-M. Li, T. He, Preparation of omniphobic PVDF membrane with hierarchical structure for treating saline oily wastewater using direct contact membrane distillation, J. Membr. Sci. 555 (2018) 197–205.
[12] E. Shaulsky, S. Nejati, C. Boo, F. Perreault, C.O. Osuji, M. Elimelech, Post-fabrication modification of electrospun nanofiber mats with polymer coating for membrane distillation applications, J. Membr. Sci. 530 (2017) 158–165.
[13] N.A.M. Barakat, M.F. Abadir, F.A. Sheikh, M.A. Kanjwal, S.J. Park, H.Y. Kim, Polymeric nanofibers containing solid nanoparticles prepared by electrospinning and their applications, Chem. Eng. J. 156 (2) (2010) 487–495.
[14] M. Khayet, C. García-Payo, T. Matsuura, Superhydrophobic nanofibers electrospun by surface segregating fluorinated amphiphilic additive for membrane distillation, J. Membr. Sci. 588 (2019), 117215.
[15] M. Essalhi, M. Khayet, Surface segregation of fluorinated modifying macromolecule for hydrophobic/hydrophilic membrane preparation and application in air gap and direct contact membrane distillation, J. Membr. Sci. 417-418 (2012) 163–173.
[16] A.K. An, J. Guo, E.-J. Lee, S. Jeong, Y. Zhao, Z. Wang, T. Leiknes, PDMS/PVDF hybrid electrospun membrane with superhydrophobic property and drop impact dynamics for dyeing wastewater treatment using membrane distillation, J. Membr. Sci. 525 (2017) 57–67.
[17] L.-F. Ren, F. Xia, J. Shao, X. Zhang, J. Li, Experimental investigation of the effect of electrospinning parameters on properties of superhydrophobic PDMS/PMMA membrane and its application in membrane distillation, Desalination 404 (2017) 155–166.
[18] Z. Chen, D. Rana, T. Matsuura, Y. Yang, C.Q. Lan, Study on the structure and vacuum membrane distillation performance of PVDF composite membranes: I, Influence of blending, Separation and Purification Technology 133 (2014) 303–312.
[19] J.A. Prince, G. Singh, D. Rana, T. Matsuura, V. Anbharasi, T. S. Shanmugasundaram, Preparation and characterization of highly hydrophobic poly (vinylidene fluoride)–Clay nanocomposite nanofiber membranes (PVDF–clay NNMs) for desalination using direct contact membrane distillation, J. Membr. Sci. 397-398 (2012) 80–86.
[20] L.D. Tijing, Y.C. Woo, W.-G. Shim, T. He, J.-S. Choi, S.-H. Kim, H.K. Shon, Superhydrophobic nanofiber membrane containing carbon nanotubes for high-performance direct contact membrane distillation, J. Membr. Sci. 502 (2016) 158–170.
[21] K. Gethard, O. Sae-Khow, S. Mitra, Water desalination using carbon-nanotube-enhanced membrane distillation, ACS Applied Materials & Interfaces 3 (2) (2011) 110–114.
[22] Y.C. Woo, L.D. Tijing, W.-G. Shim, J.-S. Choi, S.-H. Kim, T. He, E. Drioli, H.K. Shon, Water desalination using graphene-enhanced electrospun nanofiber membrane via air gap membrane distillation, J. Membr. Sci. 520 (2016) 99–110.
[23] M. Khayet, M.C. García-Payo, L. García-Fernández, J. Contreras-Martínez, Dual-layered electrospun nanofibrous membranes for membrane distillation, Desalination 426 (2018) 174–184.
[24] Y.C. Woo, L.D. Tijing, M.J. Park, M. Yao, J.-S. Choi, S. Lee, S.-H. Kim, K.-J. An, H. K. Shon, Electrospun dual-layer nonwoven membrane for desalination by air gap membrane distillation, Desalination 403 (2017) 187–198.
[25] L.D. Tijing, Y.C. Woo, M.A.H. Johir, J.-S. Choi, H.K. Shon, A novel dual-layer bicomponent electrospun nanofibrous membrane for desalination by direct contact membrane distillation, Chem. Eng. J. 256 (2014) 155–159.
[26] L. Zhao, C. Wu, X. Lu, D. Ng, Y.B. Truong, J. Zhang, Z. Xie, Theoretical guidance for fabricating higher flux hydrophobic/hydrophilic dual-layer membranes for direct contact membrane distillation, J. Membr. Sci. 596 (2020), 117608.
[27] J. Prince, D. Rana, T. Matsuura, N. Ayyanar, T. Shanmugasundaram, G. Singh, Nanofiber based triple layer hydro-philic/-phobic membrane-a solution for pore wetting in membrane distillation, Sci. Rep. 4 (2014) 6949.
[28] M. Al-Furaiji, J.T. Arena, J. Ren, N. Benes, A. Nijmeijer, J.R. McCutcheon, Triple-layer nanofiber membranes for treating high salinity brines using direct contact membrane distillation, Membranes 9 (2019) 60.
[29] L. Zhao, C. Wu, X. Lu, D. Ng, Y.B. Truong, Z. Xie, Activated carbon enhanced hydrophobic/hydrophilic dual-layer nanofiber composite membranes for high-performance direct contact membrane distillation, Desalination 446 (2018) 59–69.
[30] H.C. Yang, Y. Xie, J. Hou, A.K. Cheetham, V. Chen, S.B. Darling, Janus membranes: creating asymmetry for energy efficiency, Adv. Mater. 30 (2018) 1801495.
[31] M. Khayet, T. Matsuura, J. Mengual, Porous hydrophobic/hydrophilic composite membranes: Estimation of the hydrophobic-layer thickness, J. Membr. Sci. 266 (2005) 68–79.
[32] M. Qtaishat, M. Khayet, T. Matsuura, Guidelines for preparation of higher flux hydrophobic/hydrophilic composite membranes for membrane distillation, J. Membr. Sci. 329 (1-2) (2009) 193–200.
[33] P. Goh, A. Ismail, B. Ng, Carbon nanotubes for desalination: performance evaluation and current hurdles, Desalination 308 (2013) 2–14.
[34] M. Son, H. Park, L. Liu, H. Choi, J.H. Kim, H. Choi, Thin-film nanocomposite membrane with CNT positioning in support layer for energy harvesting from saline water, Chem. Eng. J. 284 (2016) 68–77.
[35] H. Li, W. Shi, X. Zeng, S. Huang, H. Zhang, X. Qin, Improved desalination properties of hydrophobic GO-incorporated PVDF electrospun nanofibrous composites for vacuum membrane distillation, Sep. Purif. Technol. 230 (2020), 115889.
[36] S. Li, G. Liao, Z. Liu, Y. Pan, Q. Wu, Y. Weng, X. Zhang, Z. Yang, O.K.C. Tsui, Enhanced water flux in vertically aligned carbon nanotube arrays and polyethersulfone composite membranes, J. Mater. Chem. A 2 (31) (2014) 12171–12176.
[37] J.-G. Lee, E.-J. Lee, S. Jeong, J. Guo, A.K. An, H. Guo, J. Kim, T. Leiknes, N. Ghaffour, Theoretical modeling and experimental validation of transport and separation properties of carbon nanotube electrospun membrane distillation, J. Membr. Sci. 526 (2017) 395–408.
[38] A.K. An, E.-J. Lee, J. Guo, S. Jeong, J.-G. Lee, N. Ghaffour, Enhanced vapor transport in membrane distillation via functionalized carbon nanotubes anchored into electrospun nanofibres, Scientific Reports 7 (2017) 41562.
[39] T.L.S. Silva, S. Morales-Torres, J.L. Figueiredo, A.M.T. Silva, Multi-walled carbon nanotube/PVDF blended membranes with sponge-and finger-like pores for direct contact membrane distillation, Desalination 357 (2015) 233–245.
[40] C.J. Angammana, S.H. Jayaram, Analysis of the Effects of Solution Conductivity on Electrospinning Process and Fiber Morphology, IEEE Trans. Ind. Appl. 47 (3) (2011) 1109–1117.
[41] S.-H. Tan, R. Inai, M. Kotaki, S. Ramakrishna, Systematic parameter study for ultra-fine fiber fabrication via electrospinning process, Polymer 46 (16) (2005) 6128–6134.
[42] X. Li, W. Chen, Q. Qian, H. Huang, Y. Chen, Z. Wang, Q. Chen, J. Yang, J.u. Li, Y.-W. Mai, Electrospinning-Based Strategies for Battery Materials, Adv. Energy Mater. 11 (2) (2021) 2000845, https://doi.org/10.1002/aenm.v11.210.1002/aenm.202000845.
[43] S. Huang, W.A. Yee, W.C. Tjiu, Y. Liu, M. Kotaki, Y.C.F. Boey, J. Ma, T. Liu, X. Lu, Electrospinning of polyvinylidene difluoride with carbon nanotubes: synergistic effects of extensional force and interfacial interaction on crystalline structures, Langmuir 24 (2008) 13621–13626.
[44] R.H. Magarvey, L.E. Outhouse, Note on the break-up of a charged liquid jet, J. Fluid Mech. 13 (1) (1962) 151–157.
[45] H. Fong, I. Chun, D.H. Reneker, Beaded nanofibers formed during electrospinning, Polymer 40 (16) (1999) 4585–4592.
[46] Y. Liao, C.-H. Loh, R. Wang, A.G. Fane, Electrospun superhydrophobic membranes with unique structures for membrane distillation, ACS Applied Materials & Interfaces 6 (18) (2014) 16035–16048.
[47] R. Moradi, J. Karimi-Sabet, M. Shariaty-Niassar, M. Koochaki, Preparation and characterization of polyvinylidene fluoride/graphene superhydrophobic fibrous films, Polymers 7 (8) (2015) 1444–1463.
[48] Y. Dror, W. Salalha, R.L. Khalfin, Y. Cohen, A.L. Yarin, E. Zussman, Carbon nanotubes embedded in oriented polymer nanofibers by electrospinning, Langmuir 19 (17) (2003) 7012–7020.
[49] S.-H. Wang, Y. Wan, B. Sun, L.-Z. Liu, W. Xu, Mechanical and electrical properties of electrospun PVDF/MWCNT ultrafine fibers using rotating collector, Nanoscale Research Letters 9 (2014) 1–7.

[50] M. Essalhi, M. Khayet, Self-sustained webs of polyvinylidene fluoride electrospun nanofibers at different electrospinning times: 2 Theoretical analysis, polarization effects and thermal efficiency, J. Membr. Sci. 433 (2013) 180–191.
[51] H.T. El-Dessouky, H.M. Ettouney, Fundamentals of salt water desalination, Elsevier, 2002.
[52] M. Khayet, R. Wang, Mixed matrix polytetrafluoroethylene/polysulfone electrospun nanofibrous membranes for water desalination by membrane distillation, ACS Applied Materials & Interfaces 10 (28) (2018) 24275–24287.
[53] M. Khayet, C. Cojocaru, Artificial neural network model for desalination by sweeping gas membrane distillation, Desalination 308 (2013) 102–110.
[54] M. Khayet, M. Essalhi, C. Armenta-Déu, C. Cojocaru, N. Hilal, Optimization of solar-powered reverse osmosis desalination pilot plant using response surface methodology, Desalination 261 (3) (2010) 284–292.